Article

Hydrated Alkali-Metal Cations: Infrared Spectroscopy and ab Initio Calculations of $M(HO)_2^+Ar$ cluster ions for M = Li, Na, K, and Cs

Dorothy J. Miller, and James M. Lisy

J. Am. Chem. Soc., **2008**, 130 (46), 15381-15392 • DOI: 10.1021/ja803665q • Publication Date (Web): 22 October 2008

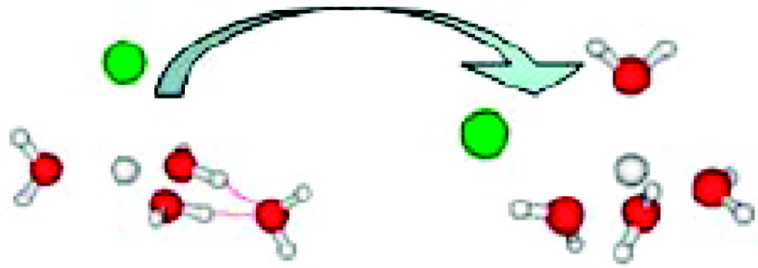

J|A|C|S
ARTICLES

Published on Web 10/22/2008

Hydrated Alkali-Metal Cations: Infrared Spectroscopy and ab Initio Calculations of $M^+(H_2O)_{x=2-5}Ar$ cluster ions for M = Li, Na, K, and Cs

Dorothy J. Miller and James M. Lisy*

Department of Chemistry, University of Illinois at Urbana−Champaign, Urbana, Illinois 61801

Received May 16, 2008; E-mail: j-lisy@uiuc.edu

Abstract: A delicate balance between competing and cooperating noncovalent interactions determines the three-dimensional structure of hydrated alkali-metal ion clusters. With a single water molecule hydrating an ion, the electrostatic ion···water interaction dominates. With more than one water molecule, however, water···water hydrogen-bonding interactions compete with the ion···water interactions to influence the three-dimensional structure. Infrared photodissociation spectra of $M^+(H_2O)_{x=2-5}Ar$ (with effective temperatures of ∼50−150 K, depending on size and composition) are reported for M = Li, Na, K, and Cs, and dependencies on ion size and hydration number are explored.

1. Introduction

Ions in an aqueous environment participate in (or influence) a number of noncovalent interactions.[1] The types and numbers of noncovalent interactions in the immediate vicinity of a hydrated ion result from a balance between ion···water and water···water interactions. This balance depends on many factors (internal energy, electron density, polarizability, etc.); however, regardless of the cluster constituents, stable geometries are those where the dominant interactions have been maximized. By systematically increasing the number of water molecules present in a hydrated cluster ion, a point where ion···water interactions are comparable to water···water interactions is reached. The cluster size where this shift in dominant noncovalent interactions occurs is ion dependent. Therefore, in order to understand how ions are solvated, it is important to study the relevant competing and cooperating noncovalent interactions in a tractable model system: one simple enough to provide molecular-level detail while still applicable to larger systems.

Gas-phase cluster ions are ideal model systems in which to probe the tipping point between specific noncovalent interactions: counterion and long-range complexities are absent, size and composition are easily controlled, structural information may be experimentally obtained, high-level ab initio computations are feasible, and ionic clusters (intermediaries between isolated species and ions in solution) can be considered molecular-level models for much larger ionic systems.[2,3] Hydration effects in these bulk systems and hydrated ion clusters can be described by a stepwise clustering of water molecules around a central cation.[4,5] Utilizing this description, a large number of theoretical[6−11] and experimental[1−4,12−21] papers (and the references therein) have investigated various aspects of ion hydration.

Binary $M^+(H_2O)_1$ (M = Li, Na, K, and Cs) cluster ions have been previously investigated and reported by this group.[22−24] The current work furthers those studies and examines competition and cooperation between noncovalent interactions in larger hydrated alkali-metal clusters. The type of noncovalent interactions, specifically, water···water hydrogen bonding present in $M^+(H_2O)_{x=2-5}Ar$ (M = Li, Na, K, and Cs) ion clusters, is explicitly examined using infrared vibrational spectroscopy. Due to the sensitivity of OH vibrations to their immediate environment, these oscillators are particularly useful probes. When an OH oscillator is perturbed by a noncovalent interaction (either ion···water and/or water···water) the frequency and intensity of that perturbed vibration is changed. How that particular mode is affected is directly related to the strength and type of the perturbing noncovalent interaction with shifts in vibrational

(1) Muller-Dethlefs, K.; Hobza, P. *Chem. Rev.* **2000**, *100* (1), 143–167.
(2) Castleman, A. W.; Bowen, K. H. *J. Phys. Chem.* **1996**, *100* (31), 12911–12944.
(3) Duncan, M. A. *Annu. Rev. Phys. Chem.* **1997**, *48*, 69–93.
(4) Coe, J. V. *Int. Rev. Phys. Chem.* **2001**, *20* (1), 33–58.
(5) Ebata, T.; Fujii, A.; Mikami, N. *Int. Rev. Phys. Chem.* **1998**, *17* (3), 331–361.
(6) Lee, H. M.; Tarakeshwar, P.; Park, J.; Kolaski, M. R.; Yoon, Y. J.; Yi, H. B.; Kim, W. Y.; Kim, K. S. *J. Phys. Chem. A* **2004**, *108* (15), 2949–2958.
(7) Schulz, F.; Hartke, B. *PCCP* **2003**, *5* (22), 5021–5030.
(8) Varma, S.; Rempe, S. B. *Biophys. Chem.* **2006**, *124* (3), 192–199.
(9) Schulz, F.; Hartke, B. *Theor. Chem. Acc.* **2005**, *114* (4−5), 357–379.
(10) Rajamani, S.; Ghosh, T.; Garde, S. *Biophys. J.* **2003**, *84* (2), 346A–346A.
(11) Rajamani, S.; Ghosh, T.; Garde, S. *J. Chem. Phys.* **2004**, *120* (9), 4457–4466.
(12) Kebarle, P. *Annu. Rev. Phys. Chem.* **1977**, *28*, 445–476.
(13) Lisy, J. M. J. *Chem. Phys.* **2006**, *125* (13), 132302.
(14) Stace, A. J. *PCCP* **2001**, *3*, 1935–1941.
(15) Duncan, M. A. *Int. J. Mass Spectrom.* **2000**, *200* (1−3), 545–569.
(16) Lisy, J. M. *Int. Rev. Phys. Chem.* **1997**, *16* (3), 267–289.
(17) Buck, U.; Huisken, F. *Chem. Rev.* **2000**, *100* (11), 3963–3890.
(18) Niedner-Schatteburg, G.; Bondybey, V. E. *Chem. Rev.* **2000**, *100* (11), 4059–4086.
(19) Robertson, W. H.; Johnson, M. A. *Annu. Rev. Phys. Chem.* **2003**, *54*, 173–213.
(20) Bieske, E. J.; Dopfer, O. *Chem. Rev.* **2000**, *100* (11), 3963–3998.
(21) Miller, D. J.; Lisy, J. M. *J. Am. Chem. Soc.* **2008**, *130*, 15393–15404.
(22) Vaden, T. D.; Forinash, B.; Lisy, J. M. *J. Chem. Phys.* **2002**, *117* (10), 4628–4631.
(23) Vaden, T. D.; Lisy, J. M.; Carnegie, P. D.; Pillai, E. D.; Duncan, M. A. *PCCP* **2006**, *8*, 3078–3082.
(24) Vaden, T. D.; Weinheimer, C. J.; Lisy, J. M. *J. Chem. Phys.* **2004**, *121* (7), 3102–3107.

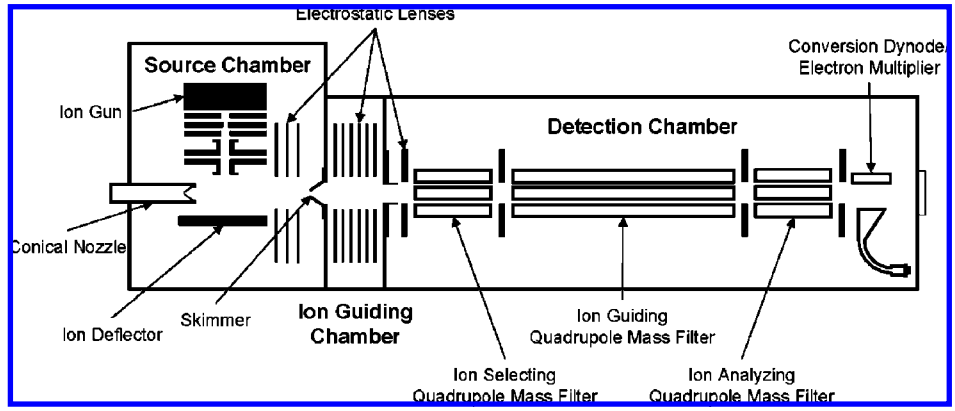

Figure 1. Experimental apparatus consisting of three pressure differential chambers: source ($\sim 10^{-3}$ Torr operational), ion guiding ($\sim 10^{-5}$ Torr operational), and detection ($\sim 10^{-8}$ Torr operational). Neutral clusters form after supersonic expansion through a 180 μm diameter conical nozzle with a backing pressure near 400 Torr. Infrared photodissociation occurs in the detection chamber if a photon from either a home-built $LiNbO_3$ optical parametric oscillator pumped by a custom 20 Hz Nd:YAG or a LaserVision OPO/OPA pumped by a 10 Hz Surelite II Nd:YAG is absorbed.

frequency ranging from a few wavenumbers for weak interactions to hundreds of wavenumbers for the strongest interactions. The binary $M^+(H_2O)_1$ study indicated that electrostatic ion···water interactions shift the OH symmetric and asymmetric stretching modes to lower frequency. The OH shift observed was indicative of the ion···water interaction strength, and thus, the magnitude of the OH frequency shift due to electrostatic perturbation increased as the ion···water interaction increased from Cs^+ to Li^+.[22−24]

Formation of an O−H···O hydrogen bond weakens the O−H covalent bond in the proton-donating water molecule and induces both a shift to lower frequency in the OH oscillator and a significant increase in the infrared (IR) intensity of the hydrogen-bonded OH feature relative to non-hydrogen-bonded OH features.[1,25] Again, the magnitude of the frequency shift depends on the strength of the hydrogen bond formed. A stronger water···water interaction perturbs the proton-donating OH oscillator more than a weaker hydrogen bond and, therefore, shifts the respective OH stretching mode lower in frequency than a weaker water···water interaction. When hydrogen bonds occur between water molecules that are also influenced by a cation, both noncovalent interactions simultaneously perturb the OH oscillator. If these perturbations are constructive, the vibrational frequency of the affected OH mode is shifted further than either perturbation would cause independently. If the simultaneous perturbations are destructive, they compete and their effect may be less than either independent perturbation.

In hydrated alkali-metal cation clusters, both electrostatic and hydrogen-bonding noncovalent interactions are present. Water molecules in the first solvation shell around the ion are polarized, leading to an increased partial positive charge on the hydrogen atoms. If that polarized water molecule then donates a proton to form a water···water hydrogen bond, the hydrogen bond formed is stronger than a hydrogen bond not enhanced by a cation. The constructive perturbations shift the associated hydrogen-bonded OH stretch lower in frequency.[14] Thus, the characteristic OH frequency shifts incited by differing noncovalent interactions provides unambiguous evidence about the type and number of interactions present in the $M^+(H_2O)_{2-5}Ar$ clusters.

2. Experimental Methods

$M^+(H_2O)_xAr$ cluster ions were generated and analyzed in the custom-built triple-quadrupole mass spectrometer shown in Figure 1. The apparatus consists of three differentially pumped chambers: a source chamber, where ion clusters are formed; an ion-guiding chamber, where ions evaporatively stabilize; and a detection chamber, where clusters are mass selected, photodissociated, and mass analyzed. In the source chamber, alkali-metal ions are generated by thermionic emission from a resistively heated, tungsten filament coated with an alkali/halide-salt impregnated paste. A supersonic expansion of argon gas with a very lean H_2O vapor content forms an ensemble of neutral $(H_2O)_xAr_y$ clusters, where $x \ll y$. The ion beam perpendicularly intersects the fully expanded molecular beam approximately 30 mm downstream from the nozzle source. Resulting ion clusters have approximately 10 eV of excess internal energy (from the collision and subsequent hydration) that is dissipated solely via evaporative cooling. As argon is the most labile species in the cluster ion, we assume that it is responsible for most, if not all, of the evaporative events.

Nascent cluster ions are imaged through a 1.0 mm aperture into the ion-guiding chamber, where the ions evaporatively stabilize. These quasi-stable ion clusters are then introduced into the detection chamber. In this chamber the species of interest is mass selected and photodissociated (following absorption of a single photon from one of two tunable infrared lasers counter propagating along the axis of the experimental apparatus) and the remaining parent cluster ions and resulting ion fragments are mass analyzed. The percent fragmentation as a function of IR frequency is reported as a predissociation cross section by correcting for the laser fluence. Absolute frequency calibration is achieved by concurrently acquiring the photoacoustic spectrum of ambient atmospheric water vapor. Reported infrared photodissociation (IRPD) spectra have been smoothed with a three-point-adjacent-averaging algorithm.

Hydrated alkali-metal cluster ions stabilize only through evaporation without collisional or three-body contributions. Over several successive evaporative events, the internal energy content of these cluster ions decreases until the time required for another evaporation event is greater than the time required to traverse the experimental apparatus. Therefore, the internal energy distributions must have an upper bound determined by the binding energy of the most weakly bound ligand, which allows the internal energy distributions of these clusters to be well characterized by the evaporative ensemble.[21,26−28] Each evaporative step removes an amount of

(25) Kozmutza, C.; Varga, I.; Udvardi, L. *J. Mol. Struct.* **2003**, *666−667*, 95–97.
(26) Cabarcos, O. M.; Weinheimer, C. J.; Lisy, J. M. *J. Phys. Chem. A* **1999**, *103*, 8777–8791.
(27) Klots, C. E. *J. Chem. Phys.* **1985**, *83* (11), 5854–5860.
(28) Klots, C. E. *Nature* **1987**, *327*, 222–223.

energy that is roughly equivalent to the argon···ion cluster interaction. After many evaporative events, this stepwise reduction of both mass and internal energy results in a quasi-stable species. Theoretical binding energies and vibrational frequencies are coupled with experimental cluster ion flight times and unimolecular dissociation rates (obtained using RRK and RRKM methods)[29−31] to estimate an effective cluster ion temperature. For the $M^+(H_2O)Ar$ (M = Li, Na, K, and Cs) cluster ions, this method predicted cluster temperatures ranging from 207 (for $Li^+(H_2O)Ar$) to 125 K (for $Cs^+(H_2O)Ar$),[21] in good agreement with experimental values.[22−24] Argon atoms are more weakly bound to the larger $M^+(H_2O)_{2-5}Ar$ clusters than to the $M^+(H_2O)_1Ar$ clusters due to a reduction in the ion···ligand pairwise interaction as the number of ligands increases. This implies that the larger $M^+(H_2O)_{2-5}Ar$ cluster ions will be colder than the $M^+(H_2O)Ar$ clusters: estimated temperatures for these larger clusters range from ∼150 to 50 K.[21]

3. Theoretical Calculations

3.1. Ab Initio Calculations. Preliminary structures were generated with Spartan 02[32] using a molecular mechanics geometry optimization with the Merck Molecular Force Field and/or an in-house Monte Carlo simulated annealing algorithm.[33] Energies and frequencies were calculated using the GAUSSIAN 03 software package.[34] Oxygen, hydrogen, and argon atoms as well as the lithium and sodium cations were treated with the augmented correlation-consistent all-electron basis set, aug-cc-pVDZ. As the aug-cc-pVDZ basis set is not available for potassium or cesium, the Los Alamos double-ζ basis sets with effective core potentials, LANL2DZ, were used for these cations.[35−37] Geometry optimization and frequency calculations were evaluated with second-order Møller−Plesset (MP2) theory to account for dispersive interactions.[1] Corrections for basis-set superposition error were neglected, as basis-set error minimally impacts relative energy differences.[38] Relative energies are reported with zero-point vibrational energy corrections (ZPE). Theoretical spectra were generated using SWizard[39] with an applied average Gaussian peak width of 20 cm^{-1}, and vibrational frequencies were scaled[40] by 0.9604 to facilitate comparison with experimental data.

3.2. Transition-State Calculations. Postulated transition-state structures were obtained by linearly interpolating the starting and ending geometries. Transition states were then located with the GAUSSIAN 03[34] software package at the MP2/6-31G theory and basis using a quadratic synchronous transit approach followed by single-point energy calculations at the larger aug-cc-pVDZ and LANL2DZ basis sets. Vibrational frequency analyses verified that optimized transition states had exactly one vibrational mode with a negative vibrational frequency.

4. Results and Discussion

Before investigating competition between electrostatic and hydrogen-bonding noncovalent interactions, these interactions need to be individually examined, starting with water···water hydrogen bonding in neutral water clusters. Cold neutral spectroscopic signatures reflect dominant water···water interactions and, therefore, serve as a reference when assigning OH spectral features in the $M^+(H_2O)_xAr$ spectra. Experimental OH signatures for neutral $(H_2O)_{1-5}$ clusters are listed in Table 1 and for $M^+(H_2O)_{1-5}Ar$ cluster ions in Table 2. These neutral signatures are important as, prior to collision with the ion, a fully expanded molecular beam consisting of neutral water/argon clusters is generated. In this initial cluster, small water clusters are expected to be suspended within a much larger argon cluster, similar to water clusters imbedded within helium droplets.[41−44]

Table 1. Observed OH Stretching Vibrations for $(H_2O)_{1-5}$ with Vibrational Mode Assignments

cluster	frequency (cm^{-1})	mode
(H_2O)[45,46]	3755.97	asym
	3657.05	sym
$(H_2O)_2$[44,47−50]	3715	asym
	3698	free
	3627	sym
	3550	HB, linear
$(H_2O)_3$[47,48,50,51]	3726	free
	3533	HB, cyclic
$(H_2O)_4$[47,48,50,52]	3720	free
	3416	HB, cyclic
$(H_2O)_5$[47,48,50,53]	3720	free
	3360	HB, cyclic

In the binary $M^+\cdots H_2O$ system, the electrostatic ion···dipole interaction shifts both the asymmetric and the symmetric vibrations lower in frequency relative to their counterparts in neutral water monomer.[22−24] While both OH stretching frequencies are affected, the electrostatic perturbation is more noticeable in the H−O−H asymmetric stretch, shifting progressively to lower frequency from Cs^+ to Li^+. The symmetric OH stretch, on the other hand, appears to be uniformly shifted (∼22 cm^{-1}) to lower frequency regardless of the magnitude of the $M^+\cdots H_2O$ interaction.[22−24]

4.1. $M^+(H_2O)_2Ar$. Water···water and ion···water interactions are in direct competition with two water molecules hydrating the cation. However, only when the water···water interaction is equivalent to or greater than the ion···water (ion···dipole) interaction will water···water hydrogen bonds form. In $M^+(H_2O)_2Ar$ clusters, the ion···water interactions are

(29) Kassel, L. S. *J. Phys. Chem.* **1928**, *32* (2), 225–242.
(30) Marcus, R. A. *J. Chem. Phys.* **1951**, *20* (3), 359–364.
(31) Rice, O. K.; Ramsperger, H. C. *J. Am. Chem. Soc.* **1927**, *49* (7), 1617–1629.
(32) Deppmeier, B. J. , et al. *SPARTAN 2002*; Wavefunction, Inc.: Irvine, CA, 2002.
(33) Nicely, A. *Ion Cluster Structure Generator 06*; Department of Chemistry, University of Illinois: Urbana, IL, 2007.
(34) Frisch, M. J., et al. *Gaussian 03, B.04*; Gaussian: Wallingford, CT, 2004.
(35) Hay, P. J.; Wadt, W. R. *J. Chem. Phys.* **1985**, *82* (1), 299–310.
(36) Wadt, W. R.; Hay, P. J. *J. Chem. Phys.* **1985**, *82* (1), 284–298.
(37) Hay, P. J.; Wadt, W. R. *J. Chem. Phys.* **1985**, *82* (1), 270–283.
(38) Lee, H. M.; Kim, J.; Lee, S.; Mhin, B. J.; Kim, K. S. *J. Chem. Phys.* **1999**, *111* (9), 3995–4004.
(39) Gorelsky, S. I. *SWizard program, 4.1*; Centre for Catalysis Research and Innovation, University of Ottawa, Ottawa, Canada, 2005.
(40) Sinha, P.; Boesch, S. E.; Gu, C.; Wheeler, R. A.; Wilson, A. K. *J. Phys. Chem. A* **2004**, *108* (42), 9213.
(41) Burnham, C. J.; Xantheas, S. S.; Miller, M. A.; Applegate, B. E.; Miller, R. E. *J. Chem. Phys.* **2002**, *117* (3), 1109–1122.
(42) Nauta, K.; Miller, R. E. *Science* **2000**, *287* (5451), 293–295.
(43) Frochtenicht, R.; Kaloudis, M.; Koch, M.; Huisken, F. *J. Chem. Phys.* **1996**, *105* (15), 6128–6140.
(44) Huang, Z. S.; Miller, R. E. *J. Chem. Phys.* **1989**, *91* (11), 6613–6631.
(45) Fraley, P. E.; Rao, K. N. *J. Mol. Spectrosc.* **1969**, *29* (1−3), 312–347.
(46) Herzberg, G. *Molecular Spectra and Molecular Structure II. Infrared and Raman Spectra of Polyatomic Molecules*; Van Nostrand Reinhold: New York, 1945.
(47) Coker, D. F.; Miller, R. E.; Watts, R. O. *J. Chem. Phys.* **1985**, *82* (8), 3554–3562.
(48) Huisken, F.; Kaloudis, M.; Kulcke, A. *J. Chem. Phys.* **1996**, *104* (1), 17–25.
(49) Page, R. H.; Frey, J. G.; Shen, Y. R.; Lee, Y. T. *Chem. Phys. Lett.* **1984**, *106* (5), 373–376.
(50) Vernon, M. F.; Lisy, J. M.; Krajnovich, D. J.; Tramer, A.; Kwok, H. S.; Shen, Y. R.; Lee, Y. T. *Faraday Discuss.* **1982**, 387–397.
(51) Pugliano, N.; Saykally, R. J. *Science* **1992**, *257* (5078), 1937–1940.
(52) Liu, K.; Brown, M. G.; Cruzan, J. D.; Saykally, R. J. *Science* **1996**, *271* (5245), 62–64.
(53) Cruzan, J. D.; Braly, L. B.; Liu, K.; Brown, M. G.; Loeser, J. G.; Saykally, R. J. *Science* **1996**, *271* (5245), 59–62.

Table 2. Experimental OH Stretching Vibrations for $M^+(H_2O)_{1\text{-}5}Ar$ (M = Li, Na, K, and Cs) Clusters with Their Vibrational Mode Assignments

cluster	frequency (cm^{-1})	mode	cluster	frequency (cm^{-1})	mode
$Li^+(H_2O)_1Ar$[23]	3696	asym	$K^+(H_2O)_4$ Ar	3710.5	asym/free
	3631	sym		3646.1	sym
$Na^+(H_2O)_1Ar$[24]	3707.0	asym		3556.2	HB, bent
	3634.5	sym	$Cs^+(H_2O)_4$ Ar	3701.1	free
$K^+(H_2O)_1Ar$[24]	3710.0	asym		3551.5	HB, cyclic
	3636.0	sym		3503.8	HB, cyclic
$Cs^+(H_2O)_1Ar$[22,24]	3711.5	asym	$Li^+(H_2O)_5Ar$	3724.9	asym/free
	3635.4	sym		3652.3	sym
$Li^+(H_2O)_2Ar$	3706.6	asym		3626.8	sym
	3637.9	sym		3547.2	HB, bent
$Na^+(H_2O)_2Ar$	3714.7	asym		3532.5	HB, bent
	3641.5	sym		3487.7	HB, linear
$K^+(H_2O)_2Ar$	3716.9	asym		3450.2	HB, linear
	3641.8	sym		3350.1	HB, linear
$Cs^+(H_2O)_2Ar$	3708.5	asym		3294.0	bend OT
	3638.2	sym	$Na^+(H_2O)_5Ar$	3718.5	asym/free
$Li^+(H_2O)_3Ar$	3720.1	asym		3652.9	sym
	3645.9	sym		3627.8	sym
$Na^+(H_2O)_3Ar$	3718.4	asym		3559.2	HB, bent
	3646.9	sym		3528.5	HB, bent
$K^+(H_2O)_3Ar$	3712.0	asym/free		3467.0	HB, linear
	3643.2	sym		3438.0	HB, linear
	3546.1	HB, bent		3368.0	HB, linear
$Cs^+(H_2O)_3Ar$	3703.3	free		3285.5	bend OT
	3529.5	HB, cyclic	$K^+(H_2O)_5Ar$	3708.1	asym/free
$Li^+(H_2O)_4Ar$	3719.7	asym/free		3647.0	sym
	3652.6	sym		3546.7	HB, bent
	3620.9	sym		3496.2	HB, bent
	3528.0	HB, bent		3453.3	HB, linear
$Na^+(H_2O)_4Ar$	3717.1	asym/free	$Cs^+(H_2O)_5Ar$	3698.6	asym/free
	3649.3	sym		3588.7	HB, bent
	3547.4	HB, bent		3547.8	HB, cyclic
				3505.2	HB, cyclic
				3461.7	HB, cyclic
				3398.1	HB, linear

Table 3. Interaction Energies (kJ/mol) for the $M^+(H_2O)_{1\text{-}2}Ar$ (M = Li, Na, K, and Cs) Cluster Constituents

	theoretical[a]		experimental
	ΔE_E	ΔE_0	$\Delta H°$
$Li^+\cdots Ar$	−23.2		−30.2[b]
$Li^+\cdots(H_2O)$	−137.2	−129.2	−142.3[c]
$Li^+(H_2O)_1\cdots Ar$	−20.1	−18.7	
$Li^+(H_2O)_1\cdots(H_2O)_1$	−123.0	−114.4	−108.0[c]
$Li^+(H_2O)_2\cdots Ar$	−11.8	−11.2	
$Na^+\cdots Ar$	−12.6		
$Na^+\cdots(H_2O)$	−93.1	−87.1	−100.4[c]
$Na^+(H_2O)_1\cdots Ar$	−11.3	−10.6	
$Na^+(H_2O)_1\cdots(H_2O)_1$	−85.1	−79.0	−82.8[c]
$Na^+(H_2O)_2\cdots Ar$	−8.2	−7.5	
$K^+\cdots Ar$			
$K^+\cdots(H_2O)$	−63.6	−58.5	−74.9[d]
$K^+(H_2O)_1\cdots Ar$	−5.5	−5.1	
$K^+(H_2O)_1\cdots(H_2O)_1$	−60.3	−55.2	−67.4[d]
$K^+(H_2O)_2\cdots Ar$	−5.6	−4.5	
$Cs^+\cdots Ar$	−3.6		−6.1[e]
$Cs^+\cdots(H_2O)$	−47.8	−43.4	−57.3[c]
$Cs^+(H_2O)_1\cdots Ar$			
$Cs^+(H_2O)_1\cdots(H_2O)_1$	−45.4	−40.9	−52.3[c]
$Cs^+(H_2O)_2\cdots Ar$	−4.6	−3.5	

[a] This work. ΔE_E and ΔE_0 are ZPE-uncorrected and ZPE-corrected binding energies, respectively. [b] Reference 54. On the basis of experimental Li^+/Ar scattering cross sections. [c] References 12 and 55. On the basis of reaction equilibrium constants. [d] References 12, 55, and 56. On the basis of reaction equilibrium constants. [e] Reference 57. On the basis of experimental Cs^+/Ar scattering cross sections.

still quite large (interaction energies are listed in Table 3), foretelling the absence of water···water hydrogen-bonded isomers. The $M^+(H_2O)_2Ar$ IRPD spectra, shown in Figure 2, are remarkably similar to the previously reported $M^+(H_2O)_1Ar$ spectra;[22−24] there is no indication of water···water hydrogen bonding.

Two non-hydrogen-bonded OH stretching features are observed: one centered near 3640 cm^{-1} and one centered near 3711 cm^{-1}. The prominent feature near 3640 cm^{-1} was identified in $M^+(H_2O)_1Ar$ clusters as the symmetric OH stretching vibration. As before, this feature shows little cation dependence, being nearly uniformly shifted (∼17 cm^{-1}) lower in frequency relative to the vibration in neutral water monomer. This shift is slightly less (Δ = 5 cm^{-1}) than that observed in the $M^+(H_2O)_1Ar$ clusters, reflecting the larger cluster size. The remaining feature (∼3711 cm^{-1}), also identified in the $M^+(H_2O)_1Ar$ spectra, is associated with asymmetric OH vibrations. The additional structure for Na^+, K^+, and Cs^+ comes from $\Delta K \pm 1$ transitions associated with this perpendicular vibrational transition. This feature, as in the monohydrated case, shows a dependency on the ion···water binding energy and shifts lower in frequency with increasing electrostatic interaction.

The similarity between the $M^+(H_2O)_2Ar$ (M = Li, Na, K, and Cs) spectra suggests that the hydrating water molecules exist in nearly identical environments. Calculated minimum energy structures, shown in Figure 3, confirm this assessment. The optimized minimum energy $M^+(H_2O)_2$ structure is linear: the cation is located in the center with a water molecule (water dipole oriented toward the cation) on either end. The weakly bound argon atom may attach to the $M^+(H_2O)_2$ cluster at various locations: in the first shell directly interacting with the cation or in the second shell interacting with a first-shell water molecule's OH group. There is no perturbation to the calculated

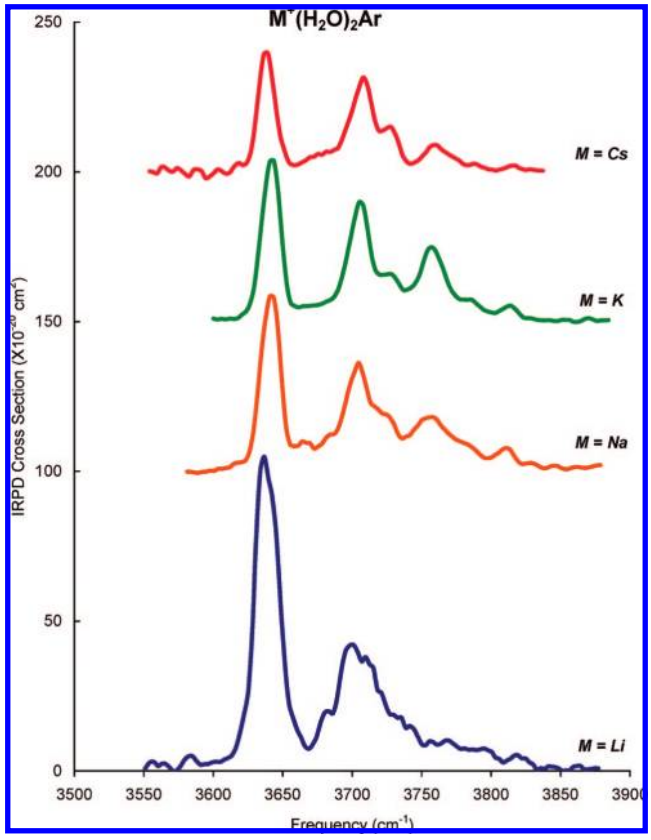

Figure 2. $M^+(H_2O)_2Ar$ IRPD spectra for M = Li, Na, K, and Cs in the free OH stretching region.

minimum energy $M^+(H_2O)_2$ structure when argon is included in the geometry optimizations; however, a slight perturbation ($\Delta = -3$ cm^{-1}) of the OH stretching frequencies is predicted if the argon atom occupies the second shell. This small shift is near the resolution limit (2 cm^{-1}) in our experimental apparatus, and therefore, Ar···H−OH interactions are unresolved. If present, such interactions may cause a slight broadening of the observed OH features.

4.2. $M^+(H_2O)_3Ar$. IRPD spectra of the $M^+(H_2O)_3Ar$ cluster ions, shown in Figure 4, exhibit a significant alkali-ion dependence. The smaller ions, Li^+ and Na^+, have spectral features similar to those observed in the dihydrated systems (Figure 2). However, the larger ions, K^+ and Cs^+, have new IR bands at lower frequencies, which indicate the onset of hydrogen bonding.

$Cs^+(H_2O)_3Ar$ clusters have the weakest electrostatic ion···ligand interactions, and as shown in Figure 4, water···water interactions dominate. Only two significant spectral features are observed: one near 3703 cm^{-1} in the non-hydrogen-bonded OH stretching region and one near 3529 cm^{-1} in the hydrogen-bonded OH region. The simplicity of this spectrum is reminiscent of the neutral water trimer spectrum, which has a hydrogen-bonded OH stretch near 3533 cm^{-1}. To attempt to identify which $Cs^+(H_2O)_3Ar$ isomer is responsible for the hydrogen-bonded signature, the structures of several low-lying isomers were identified and are shown in Figure 3. There are two hydrogen-bonded isomers that are expected to be populated under the experimental conditions: the global minimum C3a structure with two bent hydrogen bonds and the nearly isoenergetic C3b structure that has a cyclic water trimer structure. The C3c and C3d structures are present at higher energies (~10−20 times estimated thermal energies) and unlikely to be present in this ensemble of cluster ions.

As shown in Figure 5, the calculated IR spectra for the two lowest isomers appear to be in good agreement with the experimental data. Note that the bent O−H···O hydrogen-bond angles (~162°) are smaller than the preferred 180° interaction angle. This reduction in bond angle reduces the effective ion enhancement of the nominal hydrogen bond and slightly strains the hydrogen bonds. Similarly, the cyclic O−H···O hydrogen bonds are even further from linear (~129°) and, as such, are also strained interactions. However, the cesium ion does not appear to significantly impact the cyclic water structure. This is reflected in both nearly identical vibrational frequencies (3529 cm^{-1} for $Cs^+(H_2O)_3Ar$ versus 3533 cm^{-1} for $(H_2O)_3$) and similar hydrogen-bond angles (~129° for $Cs^+(H_2O)_3Ar$ versus ~139° for neutral water trimer [51]).

The hydrogen-bonded OH vibrations from both the C3a (~3545 cm^{-1}) and the C3b (~3550 cm^{-1}) isomers are within 16 and 20 cm^{-1}, respectively, of the experimentally observed hydrogen-bonded feature. Thus, an unequivocal identification of the feature near 3529 cm^{-1} cannot be made solely from the relative stabilities or the harmonic vibrational frequency analysis. As mentioned previously, the lack of a symmetric OH feature in the experimental spectrum lends indirect evidence of the C3b isomer accounting for all of the features observed in the $Cs^+(H_2O)_3Ar$ spectrum. However, it is conceivable that the spectrum is due to a mixture of the two hydrogen-bonded isomers. The implication that the slightly higher energy isomer may contribute to the OH features observed hints that this isomer may have been trapped during cluster ion formation. Further support for such dynamic trapping will be presented later in the $Li^+(H_2O)_4Ar$ cluster ion discussion, where there is a larger energetic difference between the minimum energy isomer and the experimentally observed isomer.

The non-hydrogen-bonded OH feature in the $Cs^+(H_2O)_3Ar$ spectrum (3703 cm^{-1}) is close to where the asymmetric OH vibrations have been previously identified. However, because the hydrogen-bonded feature is assigned to cyclic water···water hydrogen bonding (indicating that each water molecule is involved in two hydrogen bonds), the non-hydrogen-bonded feature comes solely from free OH oscillators. Characteristically, such free OH vibrations are narrower and slightly lower in frequency than asymmetric OH vibrations, trends clearly evident in the $Cs^+(H_2O)_3Ar$ spectrum.

In the $K^+(H_2O)_3Ar$ spectrum, a weak hydrogen-bonded feature near 3546 cm^{-1} is observed in addition to the symmetric (~3643 cm^{-1}) and asymmetric (~3712 cm^{-1}) OH stretching bands. This water···water hydrogen-bonded feature is ~17 cm^{-1} higher in frequency relative to the cyclic-type hydrogen-bonded feature identified in the $Cs^+(H_2O)_3Ar$ spectrum. As noted earlier, water···water hydrogen bonding causes the hydrogen-bonded OH stretch to shift lower in frequency as well as an increase in the IR intensity of the hydrogen-bonded feature relative to that of the non-hydrogen-bonded symmetric OH stretch. In the $K^+(H_2O)_3Ar$ spectrum the hydrogen-bonded feature (3546 cm^{-1}), while present, is much less intense than the symmetric band at 3643 cm^{-1}, which indicates that only a small percentage of the cluster ions generated populate the bent hydrogen-bonded isomer. The majority of the $K^+(H_2O)_3Ar$ clusters present assume a non-hydrogen-bonding conformation.

To help identify the water···water interactions present, four low-lying isomers of $K^+(H_2O)_3Ar$ were identified and are shown in Figure 3. The ZPE-corrected minimum energy isomer, K3a,

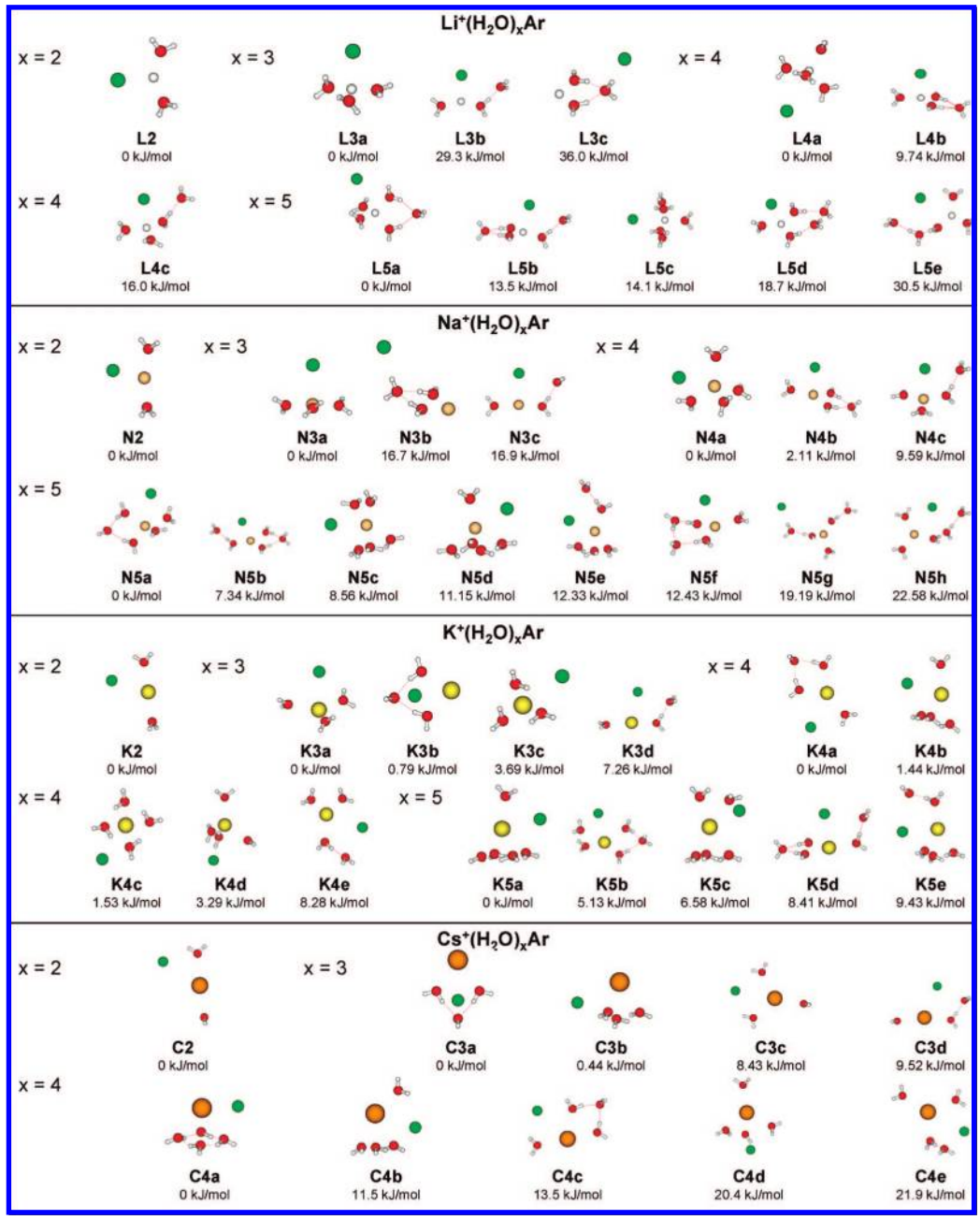

Figure 3. Low-lying structures and relative ZPE-corrected energies for $M^+(H_2O)_xAr$ for M = Li, Na, K, and Cs and $x = 2-5$. The first letter in the structure label reflects the ion. The number corresponds with the number of water molecules present in the cluster. The lower case letter indicates the relative energy ordering of that isomer (a < b < c etc.).

does not contain hydrogen bonding. To higher energy the three hydrogen-bonded isomers are located: bent (K3b, 0.79 kJ/mol), cyclic (K3c, 3.69 kJ/mol), or linear (K3d, 7.26 kJ/mol). A comparison between the experimental $K^+(H_2O)_3Ar$ spectrum and those calculated for the four low-lying isomers, shown in Figure 6, reveals good agreement between the calculated harmonic hydrogen-bonded OH vibrations from the bent $K^+(H_2O)_3Ar$ isomer and the experimentally observed feature near 3546 cm^{-1}. This suggests that two isomers are present: the K3b isomer containing a bent hydrogen bond gives rise to the weak feature near 3546 cm^{-1} and the K3a isomer lending intensity to the symmetric (~3643 cm^{-1}) and asymmetric (~3712 cm^{-1}) OH vibrations.

4.3. $M^+(H_2O)_4Ar$. Ion-dependent trends are also observed in the $M^+(H_2O)_4Ar$ spectra, which are shown in Figure 7. However, even at this larger cluster size the IRPD spectra are still relatively simple: the $Li^+(H_2O)_4Ar$, $Na^+(H_2O)_4Ar$, and $K^+(H_2O)_4Ar$ spectra all exhibit similar features (indicating similar geometries), while the $Cs^+(H_2O)_4Ar$ spectrum is noticeably different. In the $Cs^+(H_2O)_4Ar$ system, where again the weakest ion···water pairwise interactions are expected, three OH features are observed: a very prominent hydrogen-bonded band near 3503 cm^{-1}, a weak hydrogen-bonded band near 3551 cm^{-1}, and a non-hydrogen-bonded band near 3701 cm^{-1}. As in the $Cs^+(H_2O)_3Ar$ system, the symmetric OH feature is not observed, which suggests a cyclic hydrogen-bonded network. However, to unambiguously assign the observed IR bands a comparison with theoretical spectra is again necessary. Five low-lying isomers of $Cs^+(H_2O)_4Ar$ were located, the structures and relative energies of which are depicted in Figure 3. The

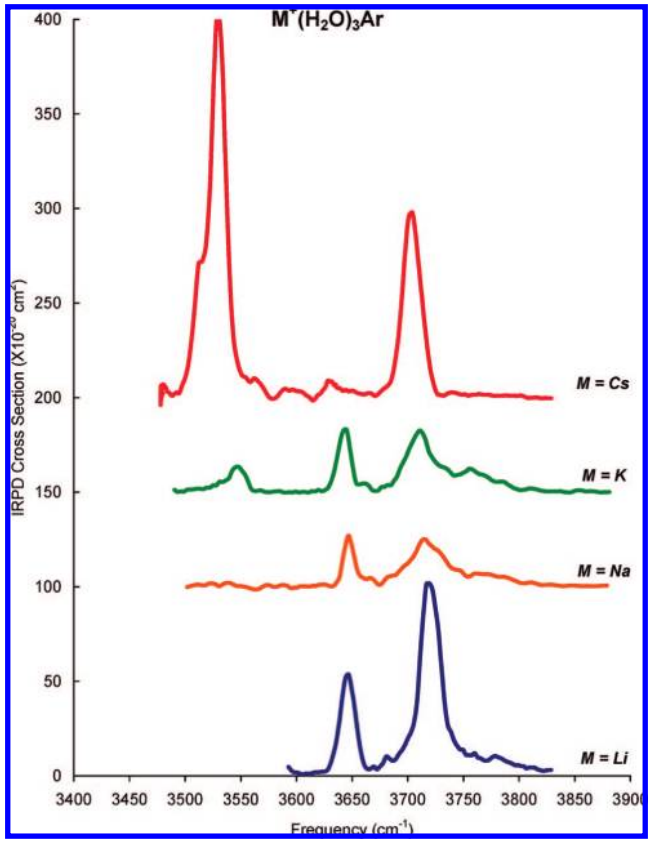

Figure 4. $M^+(H_2O)_3Ar$ IRPD spectra for M = Li, Na, K, and Cs in the free and hydrogen-bonded OH stretching regions.

minimum energy C4a conformation places the cesium cation above the plane of a hydrogen-bonded water tetramer ring. This electrostatic interaction between the ion and the cyclic moiety perturbs the O−H···O−H dihedral angle from 3° in the neutral water tetramer cluster to 65° in the $Cs^+(H_2O)_4Ar$ cluster ion. This weakens the hydrogen bonds maintaining the cyclic structure and shifts the associated hydrogen-bonded OH vibrations ~87 cm^{-1} higher in frequency relative to the hydrogen-bonded feature observed in the neutral water tetramer system. The calculated vibrational frequencies from the minimum energy isomer are in good agreement with the experimental spectrum and support the assignment of the feature near 3503 cm^{-1} to a cyclic water tetramer hydrogen bond.

Two low-lying structures could be contributing to the weak hydrogen-bonded feature near 3551 cm^{-1}: the C4b isomer (11.5 kJ/mol) and the C4c isomer (13.5 kJ/mol). These systems are nearly isoenergetic with predicted hydrogen-bonded features near 3550 cm^{-1}, thus preventing a positive assignment of the experimental feature near 3551 cm^{-1}. However, the lack of a symmetric OH feature near 3645 cm^{-1} indicates that whichever hydrogen-bonded isomer is present, it is only a very minor component of the $Cs^+(H_2O)_4Ar$ ensemble. The non-hydrogen-bonded feature near 3701 cm^{-1} can therefore be assigned primarily to free OH vibrations with only small asymmetric OH contributions.

Three OH bands are also observed in the $M^+(H_2O)_4Ar$ (M = Li, Na, and K) spectra (Figure 7): two non-hydrogen-bonded features near 3715 and 3649 cm^{-1} as well as a prominent hydrogen-bonded feature near 3556 cm^{-1} in $K^+(H_2O)_4Ar$, 3547 cm^{-1} in $Na^+(H_2O)_4Ar$, and 3528 cm^{-1} in $Li^+(H_2O)_4Ar$. The similar feature in the hydrogen-bonding region in all of the $M^+(H_2O)_4Ar$ (M = K, Na, and Li) spectra facilitates the straightforward assignment to a bent hydrogen-bonded structure. Looking at the minimum energy isomers (see Figure 3) identified for $M^+(H_2O)_4Ar$ (M = K, Na, and Li), an isomer containing bent water···water hydrogen bonding is located among the most stable conformations: in $K^+(H_2O)_4Ar$, this isomer is the minimum energy isomer (K4a); in $Na^+(H_2O)_4Ar$, the N4b isomer is nearly isoenergetic with the N4a isomer; however, in $Li^+(H_2O)_4Ar$, the L4b isomer is 9.74 kcal/mol higher in energy than the non-hydrogen-bonded, minimum energy L4a isomer. Even with larger basis sets, basis-set superposition error correction, and anharmonic vibrational frequency analysis and corrections to the ZPE (carried out by Kim et al.),[58] the $Li^+(H_2O)_4Ar$ non-hydrogen-bonded isomer is consistently predicted to be more stable than the hydrogen-bonded isomer.

As in previous instances where non-hydrogen-bonded vibrations are observed in addition to hydrogen-bonded features, the band near 3715 cm^{-1} has intensity from both asymmetric and free OH vibrations while the feature near 3649 cm^{-1} comes from the symmetric OH stretch. In the $Li^+(H_2O)_4Ar$ spectrum, two separate symmetric bands (near 3652 and 3620 cm^{-1}) are observed. These separate vibrations come from the symmetric vibrations of water molecules in different environments, namely, those in the first shell versus those in the second. In both cases the O−H bonds weaken due to noncovalent interactions; however, the magnitude of the noncovalent perturbation experienced in each case is different. The first-shell symmetric OH vibration in $Li^+(H_2O)_4Ar$ is predicted to be ~30.6 cm^{-1} higher in frequency than the second-shell OH vibration. Therefore, the higher frequency band (~3652 cm^{-1}) arises from the first-shell symmetric vibration while a second-shell symmetric vibration is responsible for the lower frequency ($\Delta = -32$ cm^{-1}) feature near 3620 cm^{-1}.

Energetically, the presence of bent hydrogen bonding in the $K^+(H_2O)_4Ar$ and to some extent in the $Na^+(H_2O)_4Ar$ spectra is supported by the computational results (although the large IR intensity of the hydrogen-bonded feature in the $Na^+(H_2O)_4Ar$ spectrum indicates that only the hydrogen-bonded isomer is present). However, in the $Li^+(H_2O)_4Ar$ spectrum hydrogen-bonded signatures were not expected since there is a measurable and consistent energetic separation between the minimum energy L4a isomer and the higher energy (9.74 kJ/mol) L4b isomer. Here, as in the $Cs^+(H_2O)_3Ar$ and $Na^+(H_2O)_4Ar$ clusters, we have an instance where a higher energy isomer is experimentally observed while the minimum energy isomer is not. When trapping the higher energy isomer was first suggested in the $Cs^+(H_2O)_3Ar$ cluster ions, sufficient support of the phenomenon was lacking: the C3a and C3b isomers are nearly isoenergetic; the bent and cyclic hydrogen-bonded features are predicted to lay in close proximity; and the IR intensity from the symmetric OH vibration may have been too weak to resolve this feature from the background noise (similar arguments may also be applied to the $Na^+(H_2O)_4Ar$ system). However, in the $Li^+(H_2O)_4Ar$ cluster ions, the hypothesis that higher energy isomers are trapped can be much better supported.

In our experiments, fully expanded neutral clusters exist prior to ion collision and hydration. When generating argon-tagged cluster ions, the neutral cluster, by necessity, must be primarily composed of argon. Coexpanding a large amount of argon gas with a small fraction of water vapor captures only a few water molecules per neutral cluster formed. These water molecules rapidly self-assemble to assume a minimum energy configuration embedded within the much larger argon cluster. When the ion

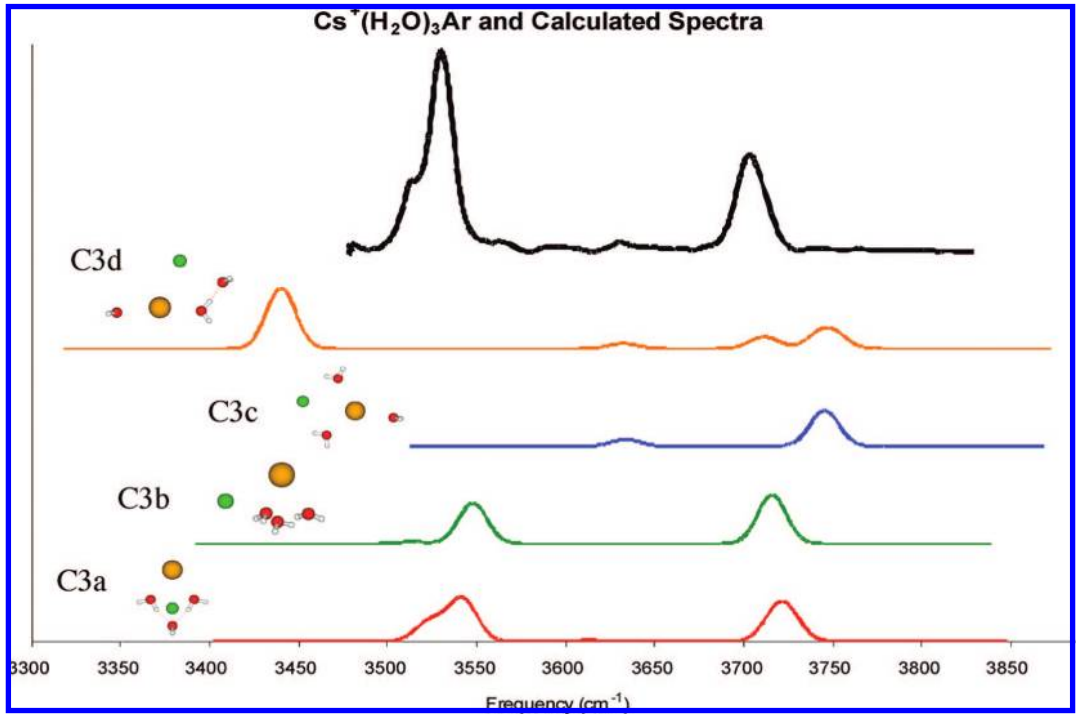

Figure 5. Experimental (top trace) and theoretical spectra (lower traces) of $Cs^+(H_2O)_3Ar$. Theoretical spectra are ordered based on ZPE-corrected relative energies from most energetically stable to least energetically stable.

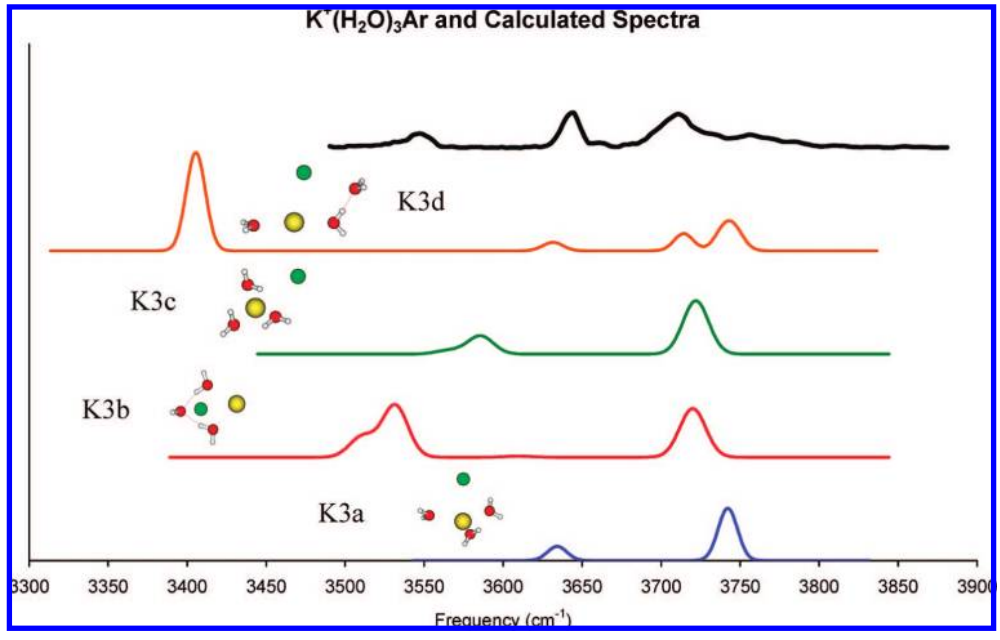

Figure 6. Experimental (top trace) and theoretical spectra (lower traces) of $K^+(H_2O)_3Ar$. The theoretical spectra are offset from the most energetically stable to least energetically stable configuration.

beam collides with these cold argon/water clusters, long-range ion···dipole interactions guide the cation through the outer argons toward the embedded water cluster. Excess energy from this collision and subsequent ion solvation is very rapidly dissipated by very efficient argon evaporation (the Ar···ion cluster interaction energy is less than 30.2 kJ/mol for the strongest Li^+···Ar interactions[54]). Such effective dissipation of excess energy leaves very little internal energy remaining to overcome subsequent barriers to cluster rearrangement: breaking pre-existing water···water hydrogen bonds to accommodate additional first shell ion···water interactions. In clusters with dominant electrostatic interactions, such as the $M^+(H_2O)_2Ar$ and the smaller $M^+(H_2O)_3Ar$ (M = Li, Na, and K) clusters,

(54) Polak-Dingels, P.; Rajan, M. S.; Gislason, E. A. *J. Chem. Phys.* **1982**, *77* (8), 3983–3993.
(55) Dzidic, I.; Kebarle, P. *J. Phys. Chem.* **1969**, *74* (7), 1466–1474.
(56) Searles, S.; Kebarle, P. *Can. J. Chem.* **1969**, *47*, 2619–2627.
(57) Rajan, M. S.; Gislason, E. A. *J. Chem. Phys.* **1982**, *78* (5), 2428–2437.
(58) Kołaski, M.; Kim, K. Personal Communiqué, 2004.

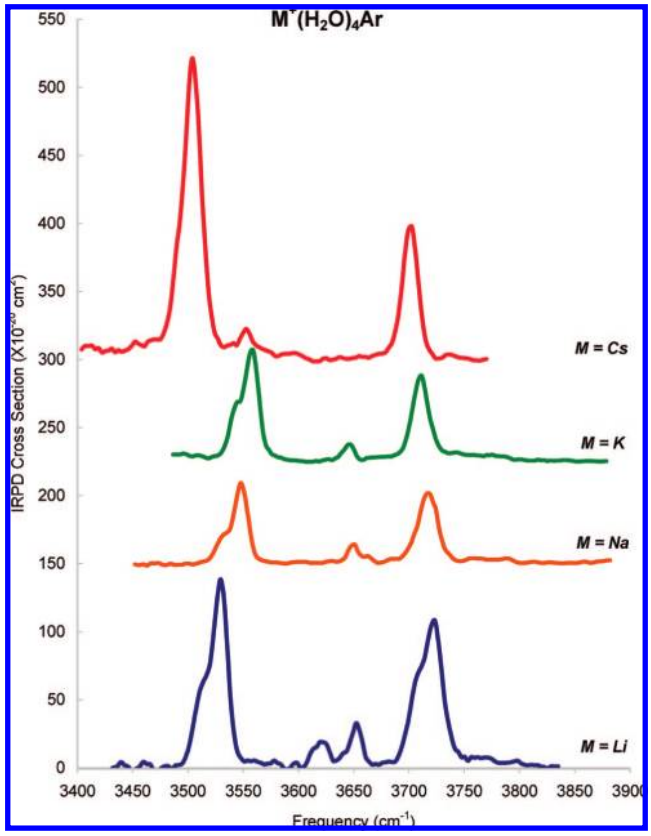

Figure 7. $M^+(H_2O)_4Ar$ IRPD spectra for M = Li, Na, K, and Cs in the free and hydrogen-bonded OH stretching regions.

water···water hydrogen bonds are broken as the ion approaches the embedded neutral water dimer or trimer. However, as the number of water molecules increases, cooperation between the hydrogen bonds increases the strength of the hydrogen-bonding interactions while the magnitude of individual ion···water electrostatic interactions decreases. In combination, this shifting balance between the competing noncovalent interactions reduces the likelihood that pre-existing hydrogen bonds will be ruptured prior to reaching a quasi-stable state, facilitating trapping of higher energy isomers during ion formation.

As discussed above, the minimum energy C4a structure dominates the $Cs^+(H_2O)_4Ar$ spectrum and, as can be seen in Figure 8, there is good agreement between the theoretical and experimental results. The other $M^+(H_2O)_4Ar$ (M = Li, Na, and K) experimental spectra suggest a different isomer is present. For K^+ and Na^+ there are several isomers within 2 kJ/mol (ca. five times thermal energy) of the ground-state configuration: K4a (0 kJ/mol), K4b (1.44 kJ/mol), and K4c (1.53 kJ/mol) for K^+ and N4a (0 kJ/mol) and N4b (2.1 kJ/mol) for Na^+. The presence of low-lying isomers containing water···water interactions suggests that the water···water interactions can now successfully compete with the ion···water interactions. However, there is little evidence of multiple isomers in the sodium or potassium experimental spectrum. In the case of $Li^+(H_2O)_4Ar$, only the L4a structure is theoretically predicted to be thermally populated. The next lowest lying isomer, L4b, is nearly 10 kJ/mol higher in energy (~20 times thermal energy), yet the spectral signatures from all three $M^+(H_2O)_4Ar$ (M = K, Na, and Li) cluster ions suggest they assume the same hydrogen-bonded structure. Therefore, there must be an additional factor in influencing the structures formed during cluster formation.

Formation of the $Cs^+(H_2O)_4Ar$ C4a structure is a barrierless process; the ion···water interaction is less favored than the water···water interaction. For the other alkali-metal cations the ion···water interaction is expected to be more favored than water···water interactions. However, these hydrated cluster ions are formed via a two-step process: first, neutral water/argon clusters are formed, and then the cation is injected. This means that existing water···water hydrogen bonds must be broken during ion hydration. As has been noted in cluster formation within helium droplets,[41−44] the efficient cooling by helium evaporation favors formation of species with low or no energetic barriers. A similar affect may be present in argon-cooled cluster ions.

We examined the case of $Li^+(H_2O)_4Ar$ to seek the answer. Starting with an optimized cyclic water tetramer cluster, a lithium cation was placed a distance two times the nominal $Li^+\cdots H_2O$ bond length at an arbitrary angle in relation to the cyclic plane. The system was then allowed to optimize without restrictions on either the cyclic tetramer or the ion. This energetic analysis of the ion···tetramer approach indicated that the breaking of two O−H···O hydrogen bonds followed by a rearrangement to the $Li^+(H_2O)_4Ar$ bent hydrogen-bonded conformation is a virtually barrierless process. However, ensuing rearrangements, either by simultaneous or sequential breaking of the remaining hydrogen bonds, as depicted in Figure 9, face a ~33.5 kJ/mol barrier. Calculated $Li^+(H_2O)_4\cdots Ar$ binding energies suggest that the argon is secured to the ion cluster by ~6 kJ/mol, well below the ~33.5 kJ/mol required for cluster rearrangement. Because the $Li^+(H_2O)_4Ar$ cluster ions are mass selected, retention of the single argon atom is guaranteed. Therefore, it is the mass selection of argon-tagged species coupled with a barrierless formation of the bent hydrogen-bonded isomer that accounts for trapping of higher energy isomers. In the three instances where higher energy isomers are observed, $Cs^+(H_2O)_3Ar$, $Na^+(H_2O)_4Ar$, and $Li^+(H_2O)_4Ar$, the trapping phenomenon discussed above supports the assignment of their respective hydrogen-bonded features solely to the higher energy isomer and, in each case, the minimum energy isomers are not present.

4.4. $M^+(H_2O)_5Ar$. The differences between the hydrogen-bonding motifs in cluster ions with larger electrostatic interactions (M = Li and Na) and those with weaker ion···water interactions (M = K and Cs) become more strikingly evident in the larger $M^+(H_2O)_5Ar$ clusters as shown in Figure 10. While features in the $K^+(H_2O)_5Ar$ spectrum can be rather straight forwardly assigned, due to the similarity with the $K^+(H_2O)_{3-4}Ar$ spectra, the remaining $M^+(H_2O)_5Ar$ (M = Li, Na, and Cs) spectra are much more complex.

Three features are present in the $K^+(H_2O)_5Ar$ spectrum: a convoluted free/asymmetric OH feature near 3708 cm^{-1}, a weak symmetric OH feature near 3647 cm^{-1}, and a prominent bent hydrogen-bonded feature near 3546 cm^{-1}. A weak feature near 3451 cm^{-1} likely comes from linear-type interactions. This interaction will be discussed in more detail in $M^+(H_2O)_5Ar$ (M = Li and Na) where structures containing this type of water···water interaction are a major component in the ensemble of cluster ions. The simplicity of this spectrum is reminiscent of the $K^+(H_2O)_4Ar$ spectrum, suggesting that the prominent hydrogen-bonded feature arises from bent water···water hydrogen bonds. However, the calculated energetic ordering of the low-lying $K^+(H_2O)_5Ar$ isomers, which are listed in Figure 3, does not locate this bent hydrogen-bonded isomer as the minimum energy configuration. An isomer with a cyclic water

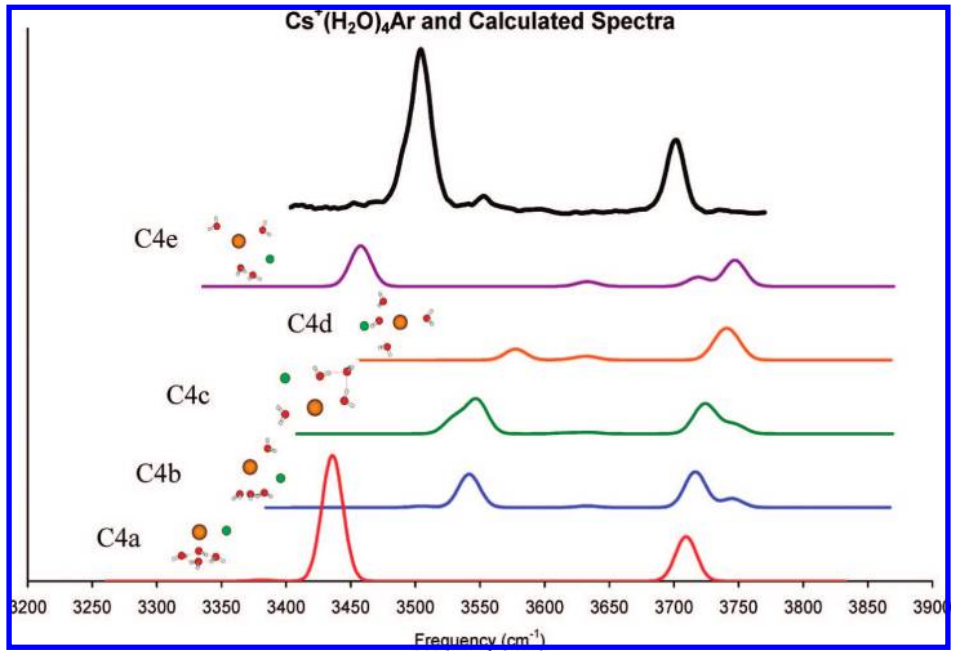

Figure 8. Experimental (top trace) and theoretical spectra (lower traces) of $Cs^+(H_2O)_4Ar$. Theoretical spectra are ordered based on ZPE corrected relative energies from most energetically stable to least energetically stable.

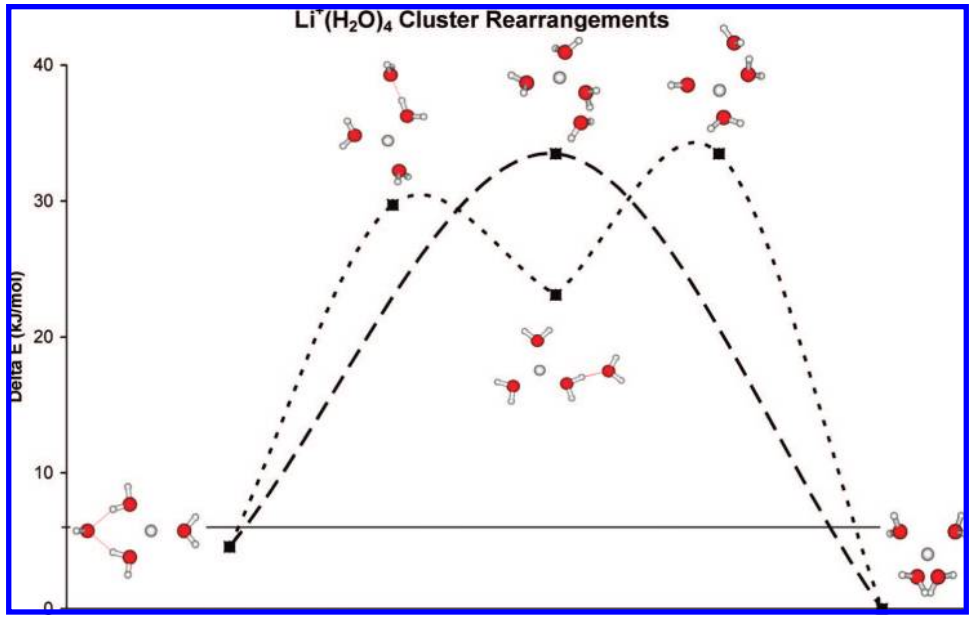

Figure 9. Energetic barriers to $Li^+(H_2O)_4Ar$ rearrangement: the solid line demarks the $Li^+(H_2O)_4\cdots Ar$ binding energy, the dashed line indicates a one-step transition from the trapped, higher energy isomer to the minimum energy isomer, and the dotted line shows a two-step rearrangement through a local minima that contains a linear water$\cdots$water interaction.

tetramer moiety is predicted to lie approximately 5 kJ/mol lower in energy, indicating that in the $K^+(H_2O)_5Ar$ system we have another instance where a higher energy isomer is trapped during cluster formation.

In the smaller $M^+(H_2O)_5Ar$ (M = Li and Na) ion clusters an unexpectedly large number of low-lying structural isomers are present, which suggests that local minimum conformations may have been trapped during cluster formation. As in earlier instances, the correlation between the $M^+(H_2O)_5Ar$ (M = Li and Na) spectra indicates that similar structural isomers contribute to both spectra. As the experimental spectra of $Li^+(H_2O)_5Ar$ and $Na^+(H_2O)_5Ar$ are nearly identical in the hydrogen-bonded region, only the $Na^+(H_2O)_5Ar$ spectrum and theoretical results will be discussed in detail. To identify hydrogen-bonded features, several low-lying isomers (Figure 3) were identified and their harmonic vibrational frequencies compared with the experimental $Na^+(H_2O)_5Ar$ spectra as shown in Figure 11. Near 3559 cm^{-1} a bent hydrogen-bonded feature is observed. A similar bent hydrogen-bonded feature was observed near 3547 cm^{-1} in the smaller $Na^+(H_2O)_4Ar$ spectrum. Now, however, this feature is broader and has a shoulder and a second band ($\sim$3526 cm^{-1}) is present. This second band suggests that similar vibrations in different environments are present with the -33 cm^{-1} shift to lower frequency, indicating that a stronger bent-type interaction has formed.

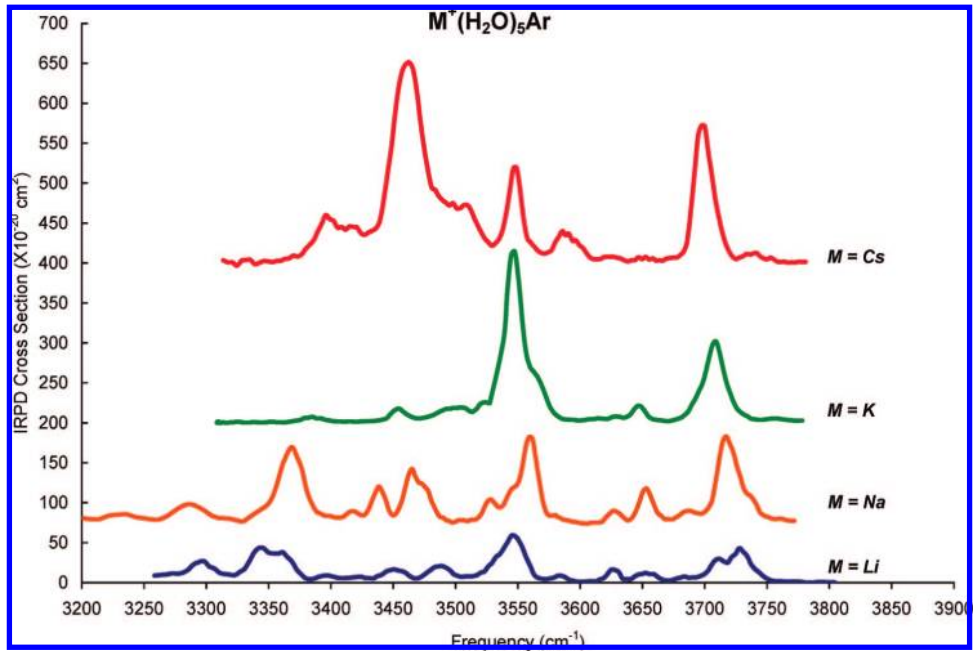

Figure 10. $M^+(H_2O)_5Ar$ IRPD spectra for M = Li, Na, K, and Cs in the free and hydrogen-bonded OH stretching regions.

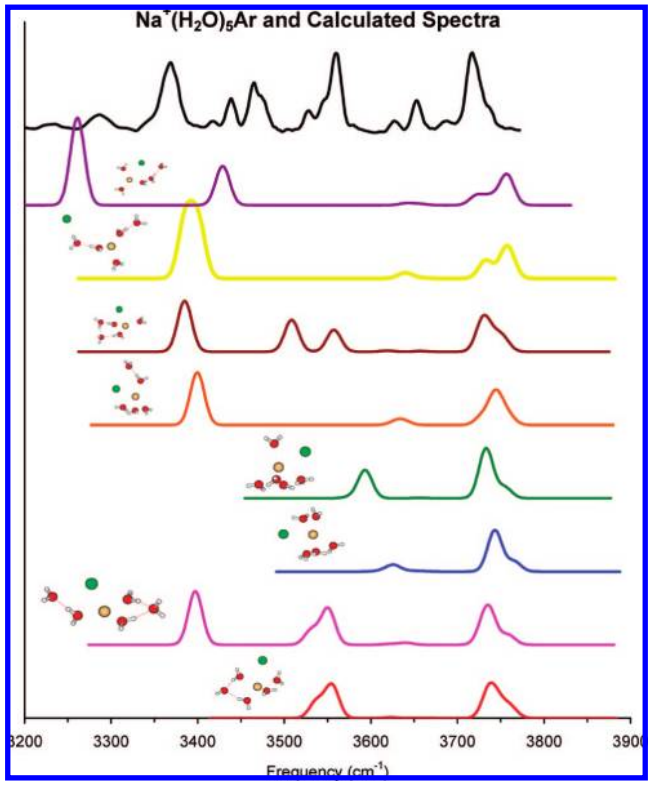

Figure 11. Experimental (top trace) and theoretical (lower traces) spectra of $Na^+(H_2O)_5Ar$. The theoretical spectra have been offset according to their ZPE relative energy ordering.

Three of the low-lying $Na^+(H_2O)_5Ar$ isomers (Figure 3) contain bent-type hydrogen bonds. As discussed previously, when similar vibrations exist in slightly different environments those oscillators will vibrate at slightly different frequencies. In the minimum energy N5a isomer four water molecules occupy positions in the first solvent shell while a proton-accepting water molecule is secured by two proton-donating first shell waters. The two higher energy isomers (N5b, 7.3 kJ/mol; N5f, 12.4 kJ/mol) have bent- and linear-type water···water interactions with only three water molecules directly interacting with the ion. This causes the bent hydrogen-bonded feature arising from these isomers to be shifted lower in frequency (4 and 46 cm^{-1}, respectively) relative to the bent vibration from the minimum energy isomer. Therefore, we can differentiate which isomer gives rise to which bent hydrogen-bonded feature: the minimum energy isomer, with the weakest bent-type interaction, gives rise to the band near 3559 cm^{-1}, while the N5b isomer adds intensity to the low-frequency side of the 3559 cm^{-1} feature, and the N5f isomer gives rise to the band near 3528 cm^{-1}.

Below 3470 cm^{-1} three features normally associated with linear-type interactions are observed: near 3467, 3438, and 3368 cm^{-1}. There is poorer agreement between the experimental and theoretical linear hydrogen-bonded vibrations; however, qualitative assignments may be made. As before, we expect the strongest linear interactions to be shifted lower in frequency relative to the weaker linear interactions. Five isomers (including the N5b and N5f isomers mentioned previously) have been identified with linear water···water hydrogen bonds: N5b (7.3 kJ/mol), N5e (12.3 kJ/mol), N5f (12.4 kJ/mol), N5g (19.2 kJ/mol), and N5h (22.6 kJ/mol). The calculated linear hydrogen-bonded OH vibrations are only slightly shifted ($\sim$15 cm^{-1}) in the four lowest energy isomers with linear-type interactions. Therefore, the features between 3420 and 3470 cm^{-1} could arise from a combination of these isomers.

The remaining prominent band near 3368 cm^{-1}, which suggests an even stronger hydrogen-bond interaction, is somewhat of a mystery. It could arise from an extended linear chain of hydrogen-bonded water molecules, and a chain that extends into the third solvent shell is present in the N5h isomer, a relatively high-energy conformer. As an alternative explanation, one of the more stable isomers, such as Nb5 with a predicted frequency of 3399 cm^{-1}, is within about 30 cm^{-1}. As noted above, the relatively poor agreement between theory and experiment for these hydrogen-bonded features and the obvious

presence of multiple isomers makes definitive assignments speculative at best.

The three higher frequency features (3725, 3652, and 3626 cm^{-1} for $Li^+(H_2O)_5Ar$ and 3718, 3653, and 3627 cm^{-1} for $Na^+(H_2O)_5Ar$) can be assigned to the non-hydrogen-bonded OH vibrations. Since hydrogen-bonded features are present (bands below 3600 cm^{-1} are associated with hydrogen-bonded OH vibrations), the feature near 3721 cm^{-1} comes from the convoluted asymmetric/free OH stretches. The two features near 3652 and 3627 cm^{-1} come from first- and second-shell symmetric OH vibrations. As before, the symmetric stretch coming from second-shell water molecules is lower in frequency than the symmetric OH stretch from first-shell water molecules.

In $Cs^+(H_2O)_5Ar$ a different set of spectral features is observed. A single non-hydrogen-bonding feature is observed near 3698 cm^{-1} that comes primarily from free OH stretches. To identify the structures associated with the features below 3600 cm^{-1}, a theoretical analysis of low-lying geometries is needed. However, due to the large number of atoms and electrons in the $Cs^+(H_2O)_5Ar$ cluster, geometry optimizations with the argon atom proved to be too computationally expensive. Therefore, the low-lying $Cs^+(H_2O)_5$ structures[21] will be used to identify likely contributors to the $Cs^+(H_2O)_5Ar$ IRPD spectrum. A comparison between the geometries and vibrational frequencies calculated for the smaller $Cs^+(H_2O)_{2-4}$ and $Cs^+(H_2O)_{2-4}Ar$ showed no difference in the structures or energetic ordering of low-lying structures or in the OH vibrational frequencies with or without an argon atom present.

Strikingly, each of the lowest lying isomers contains cyclic water···water hydrogen bonding. The calculated spectra for these isomers agree well with the more prominent (3547, 3505, and 3462 cm^{-1}) hydrogen-bonded features observed. The cyclic water trimer feature near 3547 cm^{-1} was first observed in the $Cs^+(H_2O)_3Ar$ spectrum ~15 cm^{-1} lower in frequency. This stretch is shifted higher in frequency in the $Cs^+(H_2O)_5Ar$ cluster because the reduced electrostatic ion···water interaction has a smaller perturbation on the cyclic trimer moiety. The hydrogen-bonded cyclic tetramer feature (~3505 cm^{-1}) is also shifted higher in frequency relative to $Cs^+(H_2O)_4Ar$ for the same reason. The most prominent hydrogen-bonded feature (~3462 cm^{-1}) is readily associated with a cyclic pentamer hydrogen-bonded vibration. The weak feature near 3589 cm^{-1} is near where bent hydrogen-bonded vibrations have been observed in the other $M^+(H_2O)_5Ar$ (M = K, Na, and Li) spectra. This is the first time bent hydrogen-bonded vibrations have been positively observed in the $Cs^+(H_2O)_xAr$ spectra.

5. Conclusions

We systematically probed the competition between ion···water and water···water interactions in $M^+(H_2O)_{2-5}Ar$ cluster ions. The types of hydrogen-bonding interactions observed were intricately dependent upon the ion···water interaction energy. The clusters were formed by the ion approaching a small neutral water cluster embedded in a larger argon droplet. Within the neutral droplet the pairwise water···water interactions were maximized, and with three or more water molecules neutral cyclic structures exist. For the smaller Li^+ and Na^+ cations with the strongest electrostatic interactions the ion disrupted the water···water hydrogen bonds in the neutral $(H_2O)_{2-3}$ clusters and each water molecule interacted solely with the central cation. For K^+, while the majority of $K^+(H_2O)_3Ar$ clusters had no hydrogen-bonded water molecules, a weak hydrogen-bonded feature was seen at $x = 3$, indicating that water···water interactions were becoming competitive with ion···water interactions. In $Cs^+(H_2O)_3Ar$, the weak electrostatic ion···water interactions were insufficient to disrupt the pre-existing hydrogen-bonded network. While a cyclic hydrogen-bonded isomer was predicted to be a low-lying isomer, an isomer with bent water···water interactions was predicted to be the minimum energy isomer. This was the first indication of a dynamic component (rapid argon evaporation) influencing the structures observed.

Water···water interactions are observed in all of the $M^+(H_2O)_4Ar$ (M = Li, Na, K, and Cs) ion clusters. For the hydrated cesium cation, cyclic water···water hydrogen bonding again dominated. In the smaller $M^+(H_2O)_4Ar$ (M = Li, Na, and K) clusters, stronger electrostatic interactions efficiently broke two of the existing water···water hydrogen bonds to form an isomer with bent-type hydrogen bonding. The $Li^+(H_2O)_4Ar$ spectrum provided unambiguous evidence of local minimum trapping as calculated trajectories suggested no barrier along the path from the ion···cyclic water tetramer to reach this point. There, the effective and efficient dissipation of excess internal energy by argon evaporation quenched an isomer ~10 kJ/mol above the global minimum structure. The physical reason for such trapping lays in the mass selection of $Li^+(H_2O)_4Ar$ clusters coupled with a low $Li^+(H_2O)_4$···Ar binding energy. The large barrier to subsequent cluster rearrangement precluded formation of the minimum energy isomer. This is an important consideration when applying cluster ion results to noncovalent interactions in larger systems.

Acknowledgment. This material is based on work supported in part by the National Science Foundation under grant numbers CHE-0415859 and CHE-0072178. Acknowledgment is made to the Donors of the American Chemical Society Petroleum Research Fund for partial support of this research. Our appreciation is extended to Ms. Amy Nicely, Dr. Timothy Vaden, Professor Kwang Kim, and Dr. Maciej Kołaski for their experimental and computational assistance.

Supporting Information Available: Complete refs 32 and 34. This material is available free of charge via the Internet at http://pubs.acs.org.

JA803665Q